OPEN ACCESS Freely available online

ISSN 2737-5323
Volume 4, Issue 4
https://afm.iikii.com.sg/
Applied Functional Materials

Article

Performance of Dye-sensitized Solar Cells at Different Concentrations of Graphene

Tian-Chiuan Wu[1], Tung-Lung Wu[2], Kao-Wei Min[2] Fang-Cheng Liou[1], and Teen-Hang Meen[1, *]

[1] Department of Electronic Engineering, National Formosa University, Huwei, Yunlin 632, Taiwan; eetcwu@nfu.edu.tw (T.-C. W.); xxx6577b@gmail.com (F.-C. L.)
[2] Department of Electrical Engineering, Lunghwa University of Science and Technology, Guishan District, Taoyuan City, 333, Taiwan; tunglung@gm.lhu.edu.tw (T.-L. W.); el107@gm.lhu.edu.tw (K.-W. M.)
*Corresponding author: thmeen@gs.nfu.edu.tw

Received: Nov 10, 2024; **Revised:** Nov 25, 2024; **Accepted:** Dec 02, 2024; **Published:** Dec 30, 2024

Abstract: Dye-sensitized solar cells (DSSCs) offer several advantages over traditional silicon semiconductor solar cells, including simple manufacturing processes, low cost, stable performance, and the potential for large-scale production. Graphene, known for its excellent electron transport properties and long electron lifetimes, is an ideal choice as a photoanode composite material. Graphene possesses high electrical conductivity, thermal stability, and a high specific surface area. It also has the lowest known electrical resistivity. In this study, DSSCs were fabricated using the doctor blade method by incorporating different concentrations of single-layer graphene into titanium dioxide (TiO_2). Then, the effects of various graphene concentrations on the performance of DSSCs were investigated. The addition of graphene, with its unique properties, influenced the efficiency, stability, and overall performance of DSSCs. By optimizing the concentration of graphene, the photovoltaic properties were enhanced which allows for various applications of these solar cells in various energy solutions.

Keywords: Dye-sensitized solar cells, Carbon nanotubes, Multi-walled carbon nanotubes, Titanium dioxide (TiO_2)

1. Introduction

For the development of solar cells, a variety of structures and materials are used. The evolution of solar cells has enhanced photoelectric conversion efficiency and lowered production costs. This significantly boosts the use of solar cells.

Dye-sensitized solar cells (DSSCs) were proposed in the 1970s. In 1976, H. Tsubomura and colleagues from Japan used porous zinc oxide (ZnO) as the working electrode in DSSCs, achieving a photoelectric conversion efficiency of 2.5% [1]. Such results made DSSCs a novel solar cell technology, attracting considerable academic interest. Despite this, the overall efficiency of DSSCs has shown modest improvements with significant technical challenges. As a breakthrough, Grätzel's team in Switzerland successfully sintered mesoporous, nanoscale titanium dioxide (TiO_2) particles onto a conductive substrate. Their porous nanostructured film electrode increased the electrode's specific surface area, enhancing the adsorption of ruthenium-based dyes. Coupled with an iodine/iodide (I^-/I_3^-) electrolyte, DSSCs showed a photoelectric conversion efficiency of 7.1% [2]. This significant improvement enabled titanium dioxide, ruthenium-based dyes, and iodine/iodide electrolytes to be standard materials for most DSSCs. The DSSC consists of a transparent conductive film glass, a semiconductor thin-film photoanode (working electrode), and a platinum (Pt) counter electrode. These components are assembled in a sandwich structure. The working electrode is coated with a dye, and an electrolyte is introduced into the DSSC in the assembly.

In this study, ITO glass is used as the transparent conductive substrate for the DSSCs as indium tin oxide (ITO) offers better transparency and electrical conductivity than fluorine-doped tin oxide (FTO) [3]. The lower thermal stability of ITO than FTO is not a challenge as the sintering temperature for TiO_2 is controlled at around 300°C. Temperatures exceeding 300°C can increase the resistance of the transparent conductive oxide (TCO) layer.

Carbon (C) and platinum (Pt) are the most commonly used counter-electrode materials in DSSCs [4]. In this study, platinum is selected due to its low activity, low electrical resistance, and excellent catalytic properties. Platinum also has a high oxidation potential, making it less prone to undesired reactions, which transfer electrons effectively in the reduction process. Moreover, platinum offers excellent stability and corrosion resistance [5,6], allowing it to withstand the corrosive effects of the electrolyte over extended periods. This durability extends the lifespan of the solar cell. Platinum's reflective properties are beneficial for improving the light collection efficiency of DSSCs [7], enhancing overall cell performance.

Graphene is renowned for a unique hollow structure that provides a high aspect ratio, excellent electrical conductivity, and remarkable mechanical and chemical stability [8,9]. When incorporated into TiO_2 in composite photoanodes, Graphene significantly enhances electron transport due to its high conductivity and large surface area. This incorporation improves the photocatalytic efficiency and boosts the photoelectrochemical conversion efficiency of DSSCs. Graphene is used to form a conductive network of the photoanode, facilitating efficient electron movement and reducing energy losses. In this study, we integrate graphene into DSSCs to enhance electrical conductivity and improve photocurrent generation. With the combination of TiO_2 and one-dimensional graphene, a three-dimensional conductive network is created. This network roughens the film surface and introduces additional pores to enhance dye adsorption. The increased dye uptake leads to higher light absorption and, consequently, improved photoelectric conversion efficiency. By leveraging the synergistic effects of graphene, the current limitations of DSSCs, such as poor electron transport and suboptimal light absorption can be solved. The enhanced conductive network provided by these nanomaterials allows for overcoming intrinsic inefficiencies, advancing the photovoltaic performance of DSSCs, and commercial viability. The integration of graphene enables efficient and cost-effective solar energy solutions and provides a basis for further research using advanced materials for renewable energy applications.

2. Materials and Methods

In this study, N3 dye was employed to fabricate DSSCs. The N3 dye demonstrates excellent energy gap alignment and effectively absorbs light across visible spectra from 400 to 800 nm. It features significant absorption peaks at 398 and 538 nm, and its excited state has a lifetime of up to 60 nanoseconds. We used a liquid electrolyte as it has high photoelectric conversion efficiency, rapid diffusion, and excellent penetration into porous films. The liquid electrolyte was applied in DSSCs as the $I^-/I3^-$ redox couple, providing redox reversibility and optimal stability. Ultraviolet-visible spectroscopy (UV-Vis) was used to measure the transmission and reflection of light through a sample. When light passes through a sample, lights of certain wavelengths are absorbed by the substances present in the sample. If there is a reduction or disappearance of light at specific wavelengths of a continuous spectrum, this is referred to as an absorption spectrum. The differences in absorption spectra are determined by the atoms, molecular groups, and molecules in the sample and are used for the analysis of the sample's structural characteristics and strengths.

Hitachi U2800A was used for the quantitative analysis of the samples. When electrons transition from a lower energy state to a higher energy molecular orbital, the intensity of absorbed light is recorded. Generally, ultraviolet (UV) light has a wavelength range (λ) of 200–400 nm, while visible (Vis) light ranges from 400 to 800 nm. For DSSCs, there is typically noise below 300 nm, so the instrument's wavelength range was set between 300 and 800 nm. The intensity of sunlight reaching the Earth's surface varies due to the time of day, angle of incidence, atmospheric thickness, and cloud cover. Such factors cause sunlight to be scattered or absorbed with interference from atmospheric substances. The American Society for Testing and Materials (ASTM) defines three standard solar spectra based on different angles of solar incidence: AM0, AM1, and AM1.5. The standard incident light power for solar simulation systems is AM1.5. According to international standards (IEC 891, IEC 904-1), the power density for AM1.5 is defined as 1000 W/m².

The XES-40S1 Class A solar simulation system from SAN-EI Electric was used to replicate sunlight and measure the voltage-current characteristics of the fabricated DSSCs. The solar simulation system employed a xenon lamp as the light source and the reflectors were used to adjust the light path, and multi-layer optical filters were utilized to fine-tune the wavelength intensity to accurately simulate sunlight. The simulation results allow for the detailed analysis of the solar cell's performance by examining its current-voltage output curves and overall efficiency. Key parameters include short-circuit current density (J_{SC}), open-circuit voltage (V_{OC}), fill factor (FF), photoelectric conversion efficiency (η), and maximum power (Pmax). V_{OC} stands for the maximum voltage when the solar cell circuit is open, J_{SC} indicates the maximum current density when the cell is short-circuited, Pmax represents the peak power output of the cell, and FF presents the cell's efficiency by comparing the maximum power to the theoretical power calculated from V_{OC} and J_{SC}. By providing a controlled and consistent environment to simulate sunlight, the precise evaluation of the DSSCs' performance was enabled to optimize the design and efficiency.

Incident Photon Conversion Efficiency (IPCE) was measured to estimate how efficiently photons are converted into electrons across different wavelengths of light. A spectrometer was used to isolate and generate a specific wavelength of light, which is then directed onto the experimental sample. The photocurrent generated by the sample in response to this light is converted into a voltage signal by a digital signal processor of the system. This voltage signal is then transmitted to a computer for detailed analysis. By examining the IPCE, it was determined how effectively the solar cell converts incident photons into electrical current at various wavelengths. This measurement provides data on the spectral response of the solar cell and its performance across the entire range of visible and ultraviolet light. Understanding these responses is crucial for optimizing the design and efficiency of solar cells by identifying the wavelengths at which the cell performs best and the necessary improvements. Electrochemical Impedance Spectroscopy (EIS), or AC impedance analysis, was used to investigate the electrical characteristics of a system by applying an alternating current voltage (A_{CV}) with a defined frequency and amplitude to the system. This induced a steady-state sinusoidal current response from the

system. By measuring the phase difference between the response current and the input voltage signal, EIS results were used to calculate the complex impedance of the electrode. EIS results provide information on the charge transfer resistance, capacitive behavior, and diffusion processes of the electrochemical system. By analyzing how the impedance varies with frequency, the system's behavior and performance were understood to optimize and design electrochemical cells and devices.

3. Results and Discussion

We prepared a graphene and TiO_2 composite slurry and applied them to the substrate using the doctor blade method. The surface morphology and structure of the composite film were then analyzed using FE-SEM. The graphene used had a thickness of 0.8–1.2 nm and a diameter of 0.5–2 μm. Due to its high specific surface area, graphene enhances the light absorption rate of the composite film. Additionally, its sheet-like structure provides a conductive pathway for electron transport, facilitating rapid electron transfer and reducing electron-hole recombination. Such properties improve the efficiency of DSSCs. The top view of the graphene/titanium dioxide composite film is shown in Fig. 1.

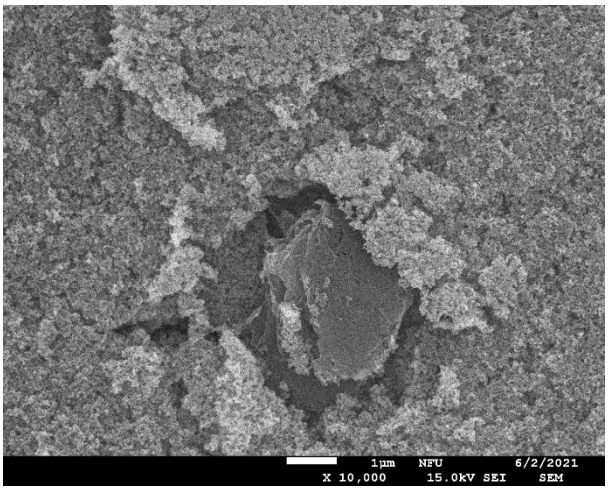

Figure 1. The top view of the graphene/titanium dioxide composite film.

Figure 2(a) shows a top view of graphene integrated with TiO_2 particles in the film. When the concentration of graphene in the slurry is too high or if the dispersion is uneven, graphene sheets can aggregate and overlap due to van der Waals forces. Figure 2(b) illustrates this aggregation of graphene, which prevents uniformly interacting with the titanium dioxide particles. Additionally, the excessive thickness of the graphene layers obstructs electron transport and increases the likelihood of electron-hole recombination. This phenomenon reduces the photoelectric conversion efficiency of DSSCs.

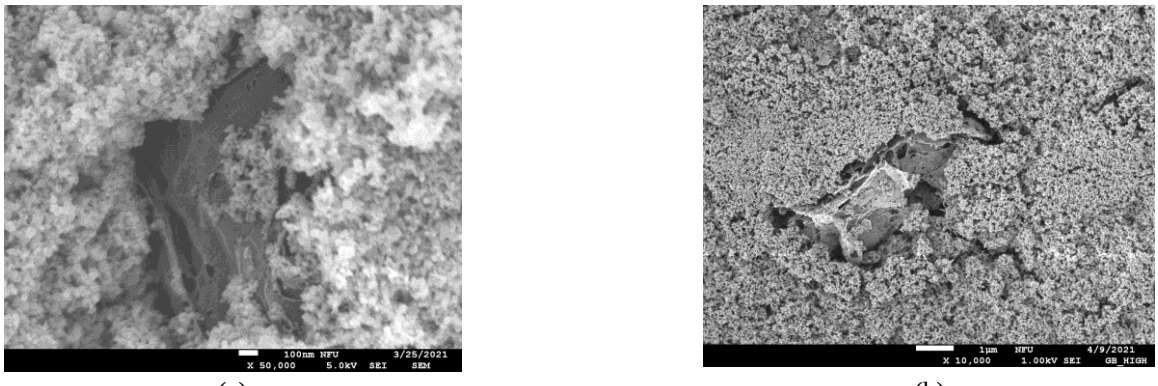

(a) (b)

Figure 2. (**a**) Top view of graphene integrated with titanium dioxide particles and (**b**) top view of graphene aggregation and overlapping.

Figure 3 shows the cross-sectional view of the graphene/TiO_2 composite film. The film became more uniform and smooth after pressing, and the thickness became more consistent. In this study, the thickness of the films after pressing was uniformly

controlled to be around 8 μm. This uniform thickness is crucial for the performance of dye-sensitized solar cells, as it ensures consistent light absorption and electron transport in the entire film. The pressing enhances the structural integrity of the composite film and improves the contact between the graphene and TiO_2 particles for efficient electron transfer. A consistent film thickness of 8 μm allows for reproducible and reliable photovoltaic performance, as variations in thickness can cause fluctuations in the cell's efficiency. By optimizing the pressing process and controlling the film thickness, high-performance and stable DSSCs were obtained which are appropriate for various practical applications.

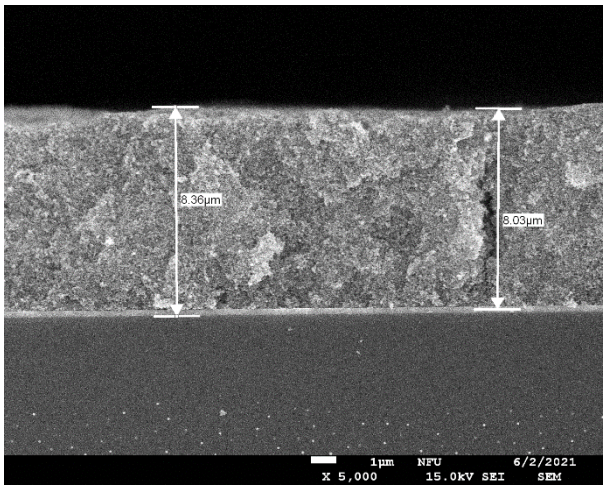

Figure 3. Cross-sectional view of the graphene/TiO_2 composite film.

Subsequently, DSSCs were fabricated using three different ratios of graphene/titanium dioxide in the composite films. The performance of these DSSCs was analyzed using J-V curves. In addition, various characterization techniques were employed, including UV-Vis absorption spectroscopy, IPCE measurements, and EIS measurements. These analyses were conducted to identify the optimal ratio of the graphene/titanium dioxide in the composite to yield the best DSSC performance. The J-V curve presents the photovoltaic parameters such as J_{SC}, V_{OC}, FF, and overall efficiency of the DSSCs. The UV-Vis absorption spectra were used to determine the light absorption properties of the composite films for maximizing photon capture. The IPCE measurement was conducted to understand the wavelength-dependent quantum efficiency of the cells and how effectively the absorbed photons were converted into electrons. EIS was used to investigate the charge transfer resistance and recombination processes at the interfaces and to understand the electronic properties and stability of the DSSCs. Based on the results, the specific concentration of graphene in the titanium dioxide matrix was found to maximize the DSSCs' efficiency and stability, which is important data for the development of high-performance solar energy devices.

The graphene concentrations used in this study were 0, 0.005, 0.01, and 0.015 wt%. Figure 4 illustrates the J-V curves for DSSCs with these varying graphene concentrations, while Table 1 presents the corresponding characteristic parameters. At a graphene concentration of 0.01 wt%, the cells showed the highest power conversion efficiency (PCE) of 3.40% and the highest short-circuit current density (J_{SC}). This enhanced performance is attributed to the flake-like structure of graphene, which provides efficient pathways for electron transport, reduces recombination losses, and improves the overall efficiency of the cells. However, when the graphene concentration increased to 0.015 wt%, both the efficiency and other parameters of the cells significantly decreased due to the increased likelihood of graphene aggregation at higher concentrations. The aggregation creates overlapping regions that hinder effective electron conduction through the graphene network. This phenomenon restricts the electrons' ability to reach the electrode, thereby reducing the overall efficiency and performance of the DSSCs. The results of this study highlight the importance of optimizing graphene concentration to enhance electron transport while minimizing aggregation effects and ensuring the optimal performance of dye-sensitized solar cells.

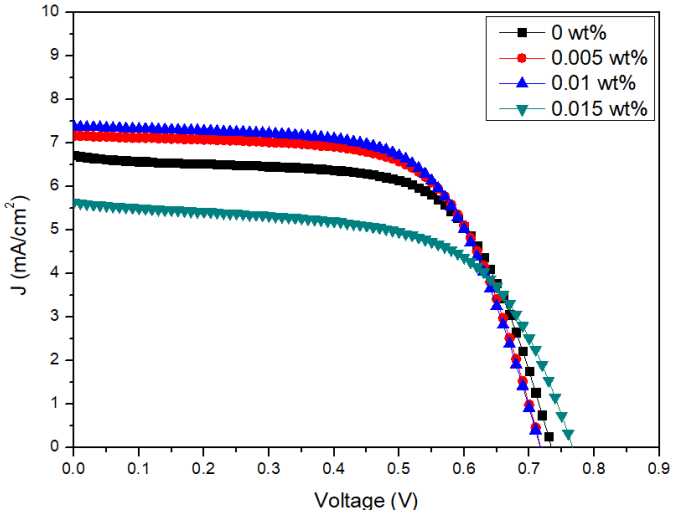

Figure 4. J-V curves for DSSCs with different graphene doping concentrations.

Table 1. J-V curve characteristic parameters for DSSCs with different graphene doping concentrations.

Concentration	Voc (V)	Jsc (mA/cm^2)	Fill Factor (%)	Efficiency (%)
0 wt%	0.73	6.71	64.75	3.19
0.005 wt%	0.72	7.17	65.33	3.36
0.01 wt%	0.72	7.37	64.30	3.40
0.015 wt%	0.77	5.64	60.80	2.63

Figure 5 shows the UV-Vis analysis result of different concentrations of graphene, and Table 2 lists their characteristic parameters. When 0.01 wt% of graphene was added to the working electrode, the dispersion effect became optimal, allowing TiO_2 to be uniformly dispersed within the working electrode, thereby increasing the amount of dye adsorption. However, an excess of graphene formed aggregation, which then hindered the light absorption of the working electrode, which decreased the light absorption efficiency. The highest light absorption for each concentration was observed between 420 and 440 nm. Due to the shorter absorption wavelength of N3 dye, there was a noticeable trend of decreasing light absorption in the longer wavelength region for all concentrations due to insufficient light absorption.

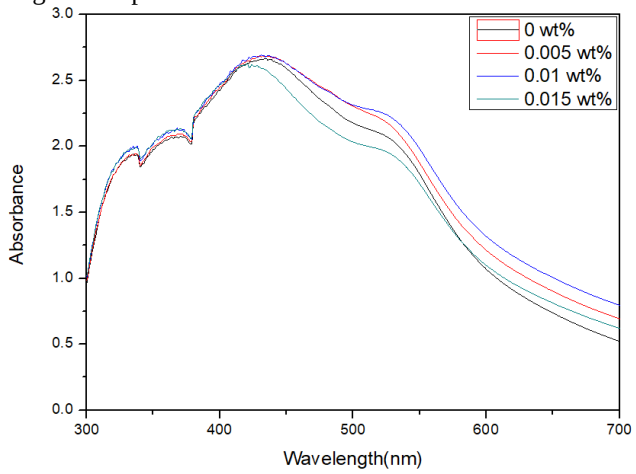

Figure 5. UV-Vis analyses of different concentrations of graphene doping.

Table 2. UV-Vis characteristics for different concentrations of graphene doping.

Concentration	Efficiency (%)	Absorbance	Wavelength (nm)
0 wt%	3.19	2.665	435
0.005 wt%	3.36	2.687	432
0.01 wt%	3.40	2.690	437
0.015 wt%	2.63	2.625	420

Figure 6 presents the IPCE analysis results at the different concentrations of graphene, while Table 3 provides the corresponding characteristic parameters. For all concentrations of graphene, efficiency was increased between 400 and 550 nm, with the highest efficiency observed between 520 and 540 nm. When the concentration was 0.01 wt%, the highest photoelectric conversion efficiency was observed. This confirmed that doping a small amount of graphene enhanced the photoinduced electron generation capability. The improvement in efficiency is attributed to better charge separation and reduced electron-hole recombination rates, as the small amount of graphene provides sufficient conductive pathways for electrons to transfer efficiently. However, when the concentration of graphene was increased beyond this optimal level, the likelihood of graphene aggregation increased. This aggregation enhanced electron-hole recombination, thereby reducing the efficiency of dye adsorption and, consequently, the overall photoelectric conversion efficiency. The findings highlight the importance of optimizing the concentration of graphene to maximize the performance of the photoelectric material, as excessive graphene is detrimental to the aggregation effects and causes the associated reduction in active surface for dye adsorption.

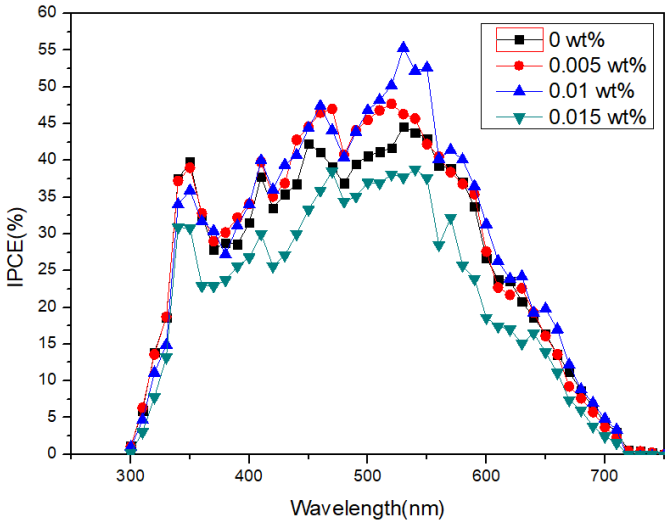

Figure 6. IPCE analyses for different concentrations of graphene doping

Table 3. IPCE characteristic parameters for different concentrations of graphene doping

Concentration	Efficiency (%)	IPCE (%)	Wavelength (nm)
0 wt%	3.19	44.62	530
0.005 wt%	3.36	47.65	520
0.01 wt%	3.40	55.30	530
0.015 wt%	2.63	38.82	540

Figure 7 shows the Nyquist plots obtained from the EIS measurements of graphene at different concentrations. The measured data are summarized in Table 4. When the graphene doping concentrations were 0.005 and 0.01 wt%, the efficiencies were as high as 3.36 and 3.40%, respectively. At a graphene concentration of 0.005 wt%, R_{pt}, R_k, and K_{eff} showed their lowest values, indicating the optimal internal resistance and the most efficient electron-hole recombination rate in the working electrode. At a concentration of 0.01 wt%, the lowest R_D and the highest efficiency were observed. As the concentration increased to 0.015 wt%, a corresponding increase in the various parameters was observed, which is attributed to the increased likelihood of graphene aggregation. This aggregation can create defects in the internal structure, preventing effective interaction with TiO_2 particles and electron transport. Consequently, the parameters deteriorated with a negative impact of excessive graphene on the material's electrochemical properties. The results underscore the importance of maintaining an optimal graphene concentration to balance the benefits of improved electron transport and the drawbacks of aggregation and structural defects.

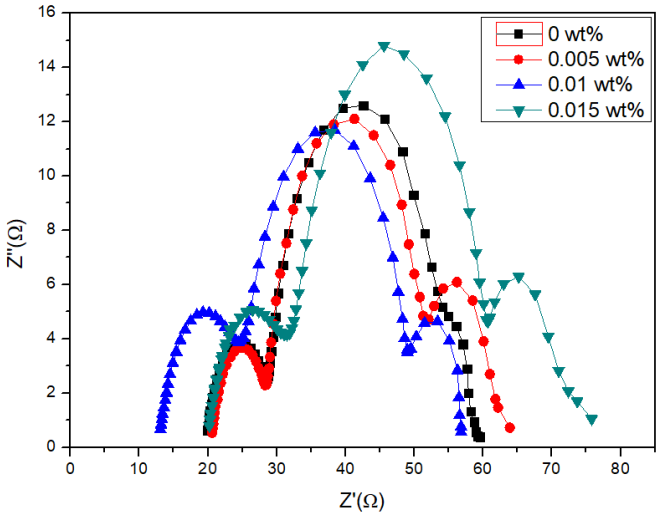

Figure 7. Nyquist plots from EIS analyses for different concentrations of graphene doping.

Table 4. 8 EIS characteristic parameters for different concentrations of graphene doping.

Concentration	Efficiency (%)	R_s (Ω)	R_{pt} (Ω)	R_k (Ω)	R_D (Ω)	K_{eff} (s^{-1})	τ_{eff} (ms)
0 wt%	3.19	19.88	8.73	25.45	5.55	25.31	39.51
0.005 wt%	3.36	20.57	7.76	23.44	12.11	19.37	51.62
0.01 wt%	3.40	13.13	11.37	24.48	7.85	25.31	39.51
0.015 wt%	2.63	20.21	11.27	29.21	15.08	32.77	30.51

4. Conclusions

We investigated the impact of varying concentrations of graphene (0, 0.005, 0.01, and 0.015 wt%) on the characteristics of DSSCs. The J-V curves showed that a graphene concentration of 0.01 wt% resulted in the highest short-circuit current density and overall efficiency. This optimal performance was consistent with different concentrations, indicating that graphene doping enhanced electron transport and reduced electron-hole recombination. The high electrical conductivity and sheet-like structure of graphene provide rapid electron transfer. Additionally, the high specific surface area of graphene increased the light absorption efficiency of the working electrode. However, as the graphene concentration increased, graphene particles tended to agglomerate. This aggregation hinders electron transport, increases electron-hole recombination rates, and ultimately decreases the efficiency of the solar cells.

Author Contributions: conceptualization, T.-C. Wu and T.-H. Meen; methodology, T.-L. Wu; validation, K.-W. Min and T.-L. Wu; formal analysis, K.-W. Min and T.-L. Wu; investigation, K.-W. Min and T.-L. Wu; resources, F.-C. Liou; data curation, F.-C. Liou; writing—original draft preparation, F.-C. Liou and K.-W. Min; writing—review and editing, F.-C. Liou; visualization, K.-W. Min; supervision, T.-C. Wu and T.-H. Meen. All authors have read and agreed to the published version of the manuscript.

Funding: This research received no external funding

Data Availability Statement: Not applicable.

Acknowledgments: The authors thank AR Display Co. Ltd., Taiwan for the financial support of this work.

Conflicts of Interest: The authors declare no conflict of interest.

References

1. Y. N. T. A.H. Tsubomura, M. Matsumura. Dye sensitised ZnO: Aqueous electrolyte: platinum photocell. *Nature* **1976**, *261*, 402–403.
2. B. O'Regan, M. Grätzel. A low-cost, high-efficiency solar cell based on dye-sensitized colloidal TiO_2 films. *Nature* **1991**, *353*, 737–739.
3. R.G. Gordon. Criteria for Choosing Transparent Conductors. *MRS Bulletin* **2000**, *25*, 52–57.
4. R. Kumar, V. Sahajwallab, P. Bhargava. Fabrication of a counter electrode for dyesensitized solar cells (DSSCs) using a carbon material produced with the organic ligand 2- methyl-8-hydroxyquinolinol (Mq). *Nanoscale Adv.* **2019**, *1*, 3192–3199.
5. M. Schwartz. *Encyclopedia of materials and finishes*, 2nd edition. CRC press: Boca Raton, FL, USA, 2002.
6. G. S. Brady, H. R. Clauser, and J. A. Vaccari. Materials handbook, 15th edition. McGraw-Hill: New York, NY, USA, 2002.

7. C. H. Yoon, R. Vittal, J. Lee, W. S. Chae, K. J. Kim. Enhanced performance of a dye-sensitized solar cell with an electrodeposited-platinum counter electrode. *Electrochim. Acta* **2008**, *53*, 2890–2896.
8. E. Muchuweni, B. S. Martincigh, V. O. Nyamori. Recent advances in graphene-based materials for dye-sensitized solar cell fabrication. *RSC Adv.* **2020**, *10*, 44453–44469.
9. M. Kokkonen, P. Talebi, J. Zhou, S. et al. Advanced research trends in dye-sensitized solar cells. *J. Mater. Chem. A.* **2021**, *9*, 10527–10545.